Coalescence of Macroscopic Flux Ropes at the Subsolar Magnetopause: Magnetospheric Multiscale Observations

M. Zhou, J. Berchem, R. J. Walker, M. El-Alaoui, X. Deng, E. Cazzola, G. Lapenta, M. L. Goldstein, W. R. Paterson, Y. Pang, R. E. Ergun, B. Lavraud, H. Liang, C. T. Russell, R. J. Strangeway, C. Zhao, B. L. Giles, C. J. Pollock, P.-A. Lindqvist, G. Marklund, F. D. Wilder, Y. V. Khotyaintsev, R. B. Torbert, and J. L. Burch

Phys. Rev. Lett. **119**, 055101 — Published 2 August 2017

DOI: 10.1103/PhysRevLett.119.055101

Coalescence of Macroscopic Flux Ropes at the Subsolar Magnetopause: Magnetospheric Multiscale Observations

M. Zhou[1], J. Berchem[1], R. J. Walker[2], M. El-Alaoui[1], X. Deng[3], E. Cazzola[4], G. Lapenta[4], M. L. Goldstein[5,12], W. R. Paterson[5], Y. Pang[3], R. E. Ergun[6], B. Lavraud[7], H. Liang[1], C. T. Russell[2], R. J. Strangeway[2], C. Zhao[2], B. L. Giles[5], C. J. Pollock[5], P-A. Lindqvist[8], G. Marklund[8], F. D. Wilder[6], Y. V. Khotyaintsev[9], R. B. Torbert[10], J. L. Burch[11]

[1] Department of Physics and Astronomy, UCLA, Los Angeles, California, USA
[2] Department of Earth, Planetary, and Space Sciences, UCLA, Los Angeles, CA, USA
[3] Nanchang University, Nanchang, P.R. China
[4] Centre for Plasma Astrophysics, Department of Mathematics, Katholieke Universiteit, Leuven, Belgium
[5] NASA, Goddard Space Flight Center, Greenbelt, Maryland, USA
[6] University of Colorado LASP, Boulder, Colorado, USA
[7] Institut de Recherche en Astrophysique et Planétologie, Université de Toulouse, CNRS, UPS, CNES, Toulouse, France
[8] Royal Institute of Technology, Stockholm, Sweden
[9] Swedish Institute of Space Physics, Uppsala, Sweden
[10] University of New Hampshire, Durham, New Hampshire, USA
[11] Southwest Research Institute, San Antonio TX, USA
[12] Space Science Institute, Boulder, CO, USA

Abstract

We report unambiguous *in-situ* observation of the coalescence of macroscopic flux ropes by the Magnetospheric Multiscale (MMS) mission. Two coalescing flux ropes with sizes of ~ 1 R_E were identified at the subsolar magnetopause by the occurrence of an asymmetric quadrupolar signature in the normal component of the magnetic field measured by the MMS spacecraft. An electron diffusion region (EDR) with width of 4 local electron inertial lengths was embedded within the merging current sheet. The EDR was characterized by an intense parallel electric field, significant energy dissipation and suprathermal electrons.

Although the electrons were organized by a large guide field, the small observed electron pressure non-gyrotropy may be sufficient to support a significant fraction of the parallel electric field within the EDR. Since the flux ropes are observed in the exhaust region, we suggest that secondary EDRs are formed further downstream of the primary reconnection line between the magnetosheath and magnetospheric fields.

Flux ropes (FRs) are magnetic structures consisting of helical field lines. They are common in space and laboratory plasmas. Examples include flux transfer events (FTE) at the magnetopause [1], plasmoids in the magnetotail [2], and coronal mass ejection (CME) flux ropes in the solar wind [3]. It has long been suggested that FRs are products of magnetic reconnection [1, 4, 5] and that they play a crucial role in the dynamics of the reconnection process by energizing particles [6] and modulating the reconnection rate [7].

Multiple FRs can be produced by multiple X-line reconnection through tearing instabilities with varying wavelengths [8]. Smaller FRs can coalesce to form larger FRs. The coalescence process has been extensively studied by numerical simulations that have shown that it is very dynamic and releases large amounts of energy [9-13]. However, direct evidence of FR coalescence in space plasmas is rare. Coalescence has been remotely observed in a CME event using STEREO spacecraft observations [14], and evidence of magnetic reconnection at the front of CME flux ropes has also been observed [3, 15]. Spacecraft observations in the Earth's magnetotail suggest that ion-scale FR coalescence occurs in the ion diffusion region [16, 17]. An outstanding question is to determine whether FRs with spatial sizes of ~100 ion inertial lengths can coalesce. It is expected that the coalescence of large FRs will have a great impact on the reconnection process because they carry large amounts of magnetic flux. Recently *Øieroset et al.* [18] identified reconnection in a single large-scale FR. While they suggested that coalescence could possibly account for the observed reconnection, they did not observe the signature of the merging of two FRs. In this letter, we present unambiguous *in-situ* evidence of ongoing macroscopic FR coalescence at Earth's magnetopause using the newly available high-resolution data from the MMS spacecraft [19]. We use these observations to investigate the microphysics of the coalescence process.

Since its launch on March 12, 2015, MMS has successfully provided electron-scale observations of the dayside magnetopause [20]. The Fluxgate Magnetometer (FGM) [21, 22], spin-plane Double Probe (SDP) and Axial Double Probe (ADP) [22-24], and Fast Plasma Instrument (FPI) [25] provide comprehensive three-dimensional measurements of the relevant fields and particles involved in magnetic reconnection.

Figure 1 presents an overview of MMS2 observations from 02:10 UT to 02:20 UT on November 17, 2015. MMS2 crossed the magnetopause around 02:14 UT at the position of [9.7, -0.9, -0.3] R_E in Geocentric Solar Magnetospheric (GSM) coordinates. Its location was very close to the subsolar magnetopause. At that time, the four MMS spacecraft formed a tetrahedron in space with a mean spacing of about 20 km. Consequently the fast survey mode data from all the spacecraft are very similar, so only data from MMS2 are plotted.

The MMS spacecraft were in the magnetosphere before 02:13:40 UT. Then they crossed the magnetopause boundary layer during the interval 02:13:40 - 02:14:40 UT (marked by the dashed orange rectangle in Figure 1). As the spacecraft entered the magnetosheath, the B_z component changed from positive to negative, plasma density increased from below 1/cm^3 up to 30/cm^3, and the ion temperature dropped from about 3 keV to 300 eV. A northward ion jet was recorded by MMS during the magnetopause crossing (Figure 1(c)). The peak speed was about 200 km/s, which is higher than the 140 km/s outflow speed expected for steady asymmetric reconnection using the parameters associated with this crossing [26]. This jet was probably a reconnection outflow produced by an X-line south of MMS. The northward jet reversed to southward with peak speed around 200 km/s on the magnetosheath side, which implies the northward motion of an X-line or the switch on (off) of reconnection northward (southward) of MMS.

Just after crossing the magnetopause, between 02:15:10 and 02:17:00 UT (dashed purple rectangle in Figure 1), MMS detected a large bipolar signature in the B_x component, which is close to the magnetopause normal component determined by a minimum variance analysis (MVA) of magnetic fields during the magnetopause crossing [27]. The magnetic field magnitude increased in association with the bipolar B_x structure. These are the typical observational signatures of a FTE at the magnetopause [1].

A remarkable feature of this event is the occurrence of a minor bipolar variation embedded within the major bipolar variation (see Figure 2(a)). Unlike the major bipolar variation in which the variation in B_x is first negative and then positive, this one is first positive then negative. Thus, the entire structure between 02:15:10 and 02:17:00 UT exhibits a quadrupolar variation in B_x. The magnitude of the central bipolar variation is smaller than that of the outer variation. Moreover, the duration of the central bipolar structure (~ 10 s) is short compared to the entire duration of the quadrupolar structure (~ 110 s). We estimated the velocity of the central bipolar structure from the values of B_x by using a four-spacecraft timing analysis [27]. We found that the central bipolar structure moved along the [0.049, 0.802, -0.595] (GSM) direction with an average speed of 45 km/s, while the local Alfvén speed was about 280 km/s and the sound speed was about 200 km/s. This means that the structure was moving mostly duskward but with a significant southward component. A single FR scenario cannot explain the observed quadrupolar signature; hence we suggest that MMS observed two FRs sequentially. There are two possible interpretations of this scenario. The first is that the two FRs were in contact without any interaction and no dissipation of magnetic energy. MMS should have recorded two successive symmetrical bipolar signatures in B_x as shown in the "non-dissipation" case in Figure 2(e). Although in this case the change in the polarity of B_x is consistent with what MMS observed, it does not reproduce the asymmetric feature of the quadrupolar structure. A more likely scenario is that the two FRs interacted in such a manner that magnetic energy was dissipated (see the "dissipation" case in Figure 2(e)), as it happens when two FRs coalesce. This would explain why MMS observed an asymmetric quadrupolar variation with the inner bipolar field weaker than the outer bipolar field as a result of the dissipation/erosion of magnetic field as a consequence of magnetic reconnection between the two FRs. We verified that the weaker and narrower inner bipolar structure observed in the magnetic field was consistent with the results of a 2-D particle-in-cell simulation of island coalescence [29].

Assuming that the two FRs were moving along the surface of the MP with speeds comparable to the ion bulk flow, we found that the northern (second) FR moved faster than the southern (first) FR. Consequently, the northern FR could catch up with the southern one, causing them to begin to merge. Furthermore, by integrating the bulk flow speed in time, we estimated that the elongation of the northern FR along the MP was about 1 $R_{E,}$ which is equivalent to 150 local ion inertial lengths d_i (given the average plasma density n = 30/cm^3). The elongation of the southern one is smaller, about 0.5 $R_E \sim 75$ d_i. The sizes of the two FRs are much larger than the ion-scale FRs that are generated by secondary instabilities in thin current layers [34].

We now relate these kinetic results to the observed microphysics of the merging current sheet. First, we construct a local LMN coordinate system by applying MVA to the magnetic field measured by MMS2 around the merging sheet. In the resulting LMN coordinate system, **N** is the normal of the merging sheet, **L** is along the reconnecting component of the two FRs and points towards the Sun, and **M** completes the right-handed orthogonal coordinate system, i.e., **M**=**N**×**L**. Figure 2(f)-2(g) illustrates the local LMN coordinates in the context of FR coalescence. **N** is consistent with the normal direction of the merging sheet we obtained by the aforementioned timing analysis.

Figure 3 details the microphysics near the merging sheet observed by MMS2. An intense current with $|J_M|$ exceeding 2μA/m^2 was detected around 02:16:08.1 UT. This current was mainly carried by electrons, as the electron bulk velocity (~ 400 km/s) was ten times larger than that of the ions (not shown). Figure 3(d)-3(f) examines the ideal conditions for both ions and electrons. Note that the profiles of $\mathbf{E}$ and $-\mathbf{V}_i\times\mathbf{B}$ deviate from each other for most of the time interval in Figure 3, indicating that the ion fluid decoupled from the magnetic field. In contrast, the profiles of $\mathbf{E}$ and $-\mathbf{V}_e\times\mathbf{B}$ track each other very well except in a narrow time interval corresponding to the intense current. The deviation between $\mathbf{E}$ and $-\mathbf{V}_e\times\mathbf{B}$ is most prominent in the $\mathbf{M}$ component as E_M reaches -6 mV/m while $(-\mathbf{V}_e\times\mathbf{B})_M$ is greater than -2 mV/m. Since B_M dominates in the merging sheet, a negative E_M gives rise to an anti-parallel electric field within the merging sheet (Figure 3(g)). The sign of E_M is consistent with the inductive reconnection electric field between two FRs according to Faraday's law. We should note that $E_{||}$ is significant only when $|E_{||}|$ is larger than the error bar (magenta shading in Figure 3(g)). Crossing the region where a significant $E_{||}$ is measured lasts about 0.09 s. Multiplying the speed of the merging sheet, we find the thickness of the $E_{||}$ region to be 4 km, which is approximately 4 d_e, where d_e is the local electron inertial length.

Figure 3(h) shows the energy dissipation in the electron rest frame $\mathbf{J}\cdot\mathbf{E}'=\mathbf{J}\cdot(\mathbf{E}+\mathbf{V}_e\times\mathbf{B})$. This quantifies the rate of non-ideal conversion of magnetic energy to plasma internal energy [35]. The strong positive peak of $\mathbf{J}\cdot\mathbf{E}'$ corresponds to the electron-scale layer. The peak value reaches about 10 nW/m^3. The energy dissipation is mainly from the parallel component, i.e., $\mathbf{J}_{||}\cdot\mathbf{E}_{||}$, while the perpendicular component is much smaller and mostly negative. The existence of significant $E_{||}$ and energy dissipation suggests that the electron-scale layer is probably the EDR of the FR coalescence. We further estimate the curl of $\mathbf{E}+\mathbf{V}_e\times\mathbf{B}$ by using the curlometer method with four spacecraft data to examine the electron frozen-in condition [36]. The result is shown in Figure 4(h). Although the uncertainty associated with this quantity is larger than the uncertainty associated with the electric field and plasma measurements, a strong peak of $|\nabla\times(\mathbf{E}+\mathbf{V}_e\times\mathbf{B})|$ is readily identified within the electron-scale layer. This is further evidence that MMS encountered an EDR [37].

Electrons show a weak non-gyrotropy within the EDR as is inferred from the measure of nongyrotropy $Q^{1/2}$ shown in Figure 3(i). It was evaluated by the formula in Ref. [38]. Although it peaks in the EDR, the peak value (~ 0.02) is smaller than the value (~ 0.1) in other EDR with negligible guide field [39]. The electron velocity distribution shown in Figure 3(k) shows that electrons are mostly organized by a large guide field ($B_g = 3.5\ B_0 \sim 70$ nT, where B_0 is the asymptotic magnetic field of the merging sheet) within the EDR. This is in contrast with the electron-scale layers in small or no guide-field cases, where the electron distribution functions are far from field-aligned due to finite Larmor radius effects or chaotic pitch-angle scattering [20, 40].

Figure 3(j) shows one snapshot of the electron pitch angle distributions (PAD) within the EDR. Enhancement of phase space densities near 90^o is clearly seen. This feature is evident in the energy range between 100 eV and 600 eV, which is about 13 times the electron temperature (see Figure 3(c)). The suprathermal electrons near 90^o are likely generated by adiabatic betatron acceleration, as the total magnetic field increases associated with the merging sheet. The effect of betatron acceleration is also evident in the local increase of electron perpendicular temperature at the EDR. Meanwhile the electron parallel temperature decreased. The mechanism leading to the parallel cooling is unknown.

Figure 4 presents the four spacecraft observations around the EDR. Data from MMS1, MMS3 and MMS4 has been shifted by 0.46 s, 0.16 s and 0.04 s, so that the observations of the EDR are aligned. All four spacecraft detected negative B_N and positive v_{eL} in the vicinity of the merging sheet. This suggests that the MMS spacecraft were sunward of the merging line. v_{eL} changed to negative after crossing the merging sheet. Based on the observed flow variations we inferred the electron flow structure as depicted in Fig. 2(g). This is consistent with the electron flows in guide field reconnection [41]. $\mathbf{J}\cdot\mathbf{E}$□ measured by MMS1 and 2 are similar, and are much stronger than those measured by MMS3 and 4. This can be understood from the four spacecraft configuration in space. MMS1 was 4 km from MMS2 in the –**L** direction, while MMS4 and MMS3 were 12 km and 19 km apart respectively from

MMS2 in the +**L** direction. This implies that the EDR was also localized in the L direction as MMS1 and 2 detected the EDR while MMS3 and 4 were outside the EDR (see the schematic in Figure 2(g)). Assuming the aspect ratio of the EDR was 0.1 (which equals the dimensionless reconnection rate), the extent of the EDR was about 40 km in L given the full width of the EDR was 4 km. If MMS4 skimmed the edge of the EDR, then MMS2 and MMS1 were about 8 d_e and 4 d_e from the merging line, respectively.

Finally, we roughly estimate the magnitudes of the non-ideal terms in the electron momentum equation. The inertial term in the M direction can be written as $\frac{m_e}{e}\frac{d\vec{v}_e}{dt} \approx \frac{m_e}{e}(\vec{v}_e \cdot \nabla)\vec{v}_e \sim \frac{m_e}{e}\frac{v_{eN}\Delta v_{eM}}{d_e}$ by assuming that the gradient along the N direction is dominant over the other two directions. The temporal variation is neglected because there is no significant variation in the flow enhancement as the EDR moved from MMS1 to MMS2. We can estimate that the gradient length of the electron flow (v_{eM}) in the EDR along the normal direction is comparable to $d_e \sim 1$ km. Given that $v_{eN} \sim 100$ km/s and $\Delta v_{eM} \sim 400$ km/s then the contribution from the inertial term is nearly 0.3 mV/m.

The electron pressure gradient term contributed by the off-diagonal pressure terms can be written as $\left(\frac{\nabla \cdot \overline{\overline{\mathrm{P}}}_e}{\mathrm{n_e e}}\right)_{\mathrm{M}} = \left(\frac{\partial P_{LM}}{\partial L} + \frac{\partial P_{MN}}{\partial N}\right)/n_e e \sim \frac{\Delta \mathrm{P_{MN}}}{\mathrm{d_e} n_e e}$. Even though electrons were organized by a large guide field, the off-diagonal terms in the electron pressure tensor are not negligible because of the existence of non-gyrotropy. We can estimate their contribution by assuming that the gradient length is the electron inertial length. Given that $\Delta P_{MN} \approx 0.015$ nPa and $d_e \sim 1$ km, then the contribution is nearly 3 mV/m. The above estimate suggests that pressure non-gyrotropy is more important than electron inertial in supporting $E_{||}$ in the EDR. This is different than the case for an EDR in large guide field reconnection reported from MMS [42] which suggests that $E_{||}$ was balanced by a combination of electron inertial and parallel gradient of gyrotropic electron pressure.

In summary, we provide the first *in-situ* observations of macroscopic FR coalescence at the Earth's magnetopause. Our identification is based on the following criteria: 1) the observation of an asymmetric quadrupolar structure indicating dissipation between two FRs; 2) the agreement between plasma/field characteristics of the two interacting FRs and magnetic reconnection signatures.

In-situ observation of FR coalescence provides us with the opportunity to have a better understanding of the coalescence process. We show that the coalescence involved a multi-scale process: energy injected from the fluid-scale merging of the FRs was subsequently dissipated at the electron-scale in the EDR. Our study shows that the coalescence of macroscopic FRs can provide significant energy dissipation in addition to that at the primary reconnection site. We expect that multiple reconnection sites would form along the direction of the FRs' axes as shown in Figure 2(f), thus FR coalescence may be important for energy transport in solar wind-magnetosphere coupling. Furthermore, since both FRs were observed within a reconnection jet, our analysis shows that secondary EDRs can form further downstream from the primary X-line. Hence, FR coalescence could provide MMS more opportunities for exploring electron physics in EDRs than was originally thought.

We thank T. Phan and N. Bessho for valuable suggestions. This research was supported by NASA Magnetospheric Multiscale Mission Interdisciplinary Scientist grant NNX08AO48G, NASA grant NNX15AI92G and NSF grant AGS-1450864. Work in China was supported by the National Natural Science Foundation of China (NSFC) under grants 41331070 and 41522405 and Science Foundation of Jiangxi Province (Grant No. 20142BCB23006). EC acknowledges financial support from the Leverhulme Trust Research Project Grant No. 2014-112. We thank the entire MMS team and instrument PIs for data access and support. The MMS data can be accessed from MMS Science Data Center (https://lasp.colorado.edu/mms/sdc/public/)

Reference

[1] Russell, C. T., and R. C. Elphic, Space Sci. Rev., 22, 681-715 (1978).

[2] Zong, Q.-G., et al., Geophys. Res. Lett., 31, L18803, doi:10.1029/2004GL020692 (2004).

[3] Ruffenach, A., B. Lavraud, M. J. Owens, J.-A. Sauvaud, N. P. Savani, A. P. Rouillard, P. Démoulin, C. Foullon, A. Opitz, A. Fedorov, Jacquey, V. Génot, P. Louarn, J. G. Luhmann, C. T. Russell, C. J. Farrugia, and A. B. Galvin, J. Geophys. Res., 117, A09101, doi:10.1029/2012JA017624 (2012)

[4] Lee, L. C., and Z. F. Fu, Geophys. Res. Lett., 12, 105–108 (1985)

[5] Slavin, J. A., R. P. Lepping, J. Gjerloev, D. H. Fairfield, M. Hesse, C. J. Owen, M. B. Moldwin, T. Nagai, A. Ieda, and T. Mukai, J. Geophys. Res., 108(A1), 1015, doi:10.1029/2002JA009557 (2003).

[6] Drake, J. F., M. Swisdak, H. Che, and M. A. Shay, Nature, 443(7111), 553–556 (2006)

[7] Karimabadi, H., W. Daughton, and J. Scudder, Geophys. Res. Lett., 34, L13104, doi:10.1029/2007GL030306 (2007)

[8] Daughton,W., J. Scudder, and H. Karimabadi, Phys. Plasmas, 13, 072101, doi:10.1063/1.2218817 (2006)

[9] Richard, R. L., R. J. Walker, R. D. Sydora, *and* M. Ashour-Abdalla, J. Geophys. Res., 94(A3), 2471–2483, *doi:*10.1029/JA094iA03p02471 (1989).

[10] Cazzola, E., M. E. Innocenti, S. Markidis, M. V. Goldman, D. L. Newman, and G. Lapenta, Physics of Plasmas (1994-present), 22 (9), 092,901 (2015)

[11] Oka, M., T. D. Phan, S. Krucker, M. Fujimoto, and I. Shinohara, Astrophys. J., 714, 915–926, doi:10.1088/0004-637x/714/1/915 (2010).

[12] P. L. Pritchett, Phys. Plasmas 14, 052102 (2007).

[13] Zhou, M., Y. Pang, X. Deng, S. Huang, and X. Lai, J. Geophys. Res. Space Physics, 119, doi:10.1002/2013JA019483 (2014).

[14] Song, H.Q., Y. Chen, G. Li, and X. L. Kong, Phys. Rev. X, 2, 021015 (2012).

[15] Lavraud, B., A. Ruffenach, A. P. Rouillard, P. Kajdic, W. B. Manchester, and N. Lugaz, , J. Geophys. Res. Space Physics, 119, doi:10.1002/2013JA019154, 2014; Ruffenach, A., B. Lavraud, C. J. Farrugia, P. Démoulin, S. Dasso, M. J. Owens, J.-A. Sauvaud, A. P. Rouillard, A. Lynnyk, C. Foullon, N. P. Savani, J. G. Luhmann, and A. B. Galvin, J. Geophys. Res., 120, doi:10.1002/2014JA020628, 2015.

[16] Retinò, A., et al., J. Geophys. Res., 113, A12215, doi:10.1029/2008JA013511 (2008).

[17] Wang, R., Q. Lu, R. Nakamura, C. Huang, A. Du, F. Guo, W. Teh, M. Wu, S. Lu, and S. Wang, Nature Physics, Vol. 12, doi: 10.1038/NPHYS3578 (2015).

[18] Øieroset, M., et al., Geophys. Res. Lett., 43, 5536–5544, doi:10.1002/2016GL069166 (2016).

[19] Burch, J. L., et al., Space Sci. Rev., 199, 5–21, doi:10.1007/s11214-015-0164-9 (2016).

[20] Burch, J. L., et al., Science, doi:10.1126/science.aaf2939 (2016); Burch, J. L. and T. D. Phan, Geophys. Res. Lett., 43, doi:10.1002/2016GL069787 (2016).

[21] Russell, C. T., et al., Space Sci Rev, 199(1-4), 189-256, doi:10.1007/s11214-014-0057-3 (2016).

[22] Torbert, R. B., et al., Space Sci. Rev., 199, 105–135, doi:10.1007/s11214-014-0109-8 (2016).

[23] Lindqvist, P.-A., et al., Space Sci. Rev., 199, 137–165, doi:10.1007/s11214-014-0116-9 (2016).

[24] Ergun, R. E., et al., Space Sci. Rev., 199, 167–188, doi:10.1007/s11214-014-0115-x (2016)

[25] Pollock, C. J., et al., Space Sci. Rev., 199, 331–406, doi:10.1007/s11214-016-0245-4 (2016).

[26] Cassak, P. A., and M. A. Shay, *Phys. Plasmas*, 14, 102114 (2007).

[27] Sonnerup, B. U. O. and M. Scheible, no. SR-001 in ISSI Scientific Reports, Chap. 1, pp. 185-220, ESA Publ. Div., Noordwijk, Netherlands (1998).

[28] Sonnerup, B. U. O., S. E. Haaland and G. Paschmann, no. SR-008 in ISSI Scientific Reports, Chap. 1, pp. 1-15, ESA Publ. Div., Noordwijk, Netherlands (2008).

[29] See Supplemental Material at [url] for details on the PIC simulation of island coalescence, which includes Refs. [30-33].

[30] Markidis, S., G. Lapenta, and R. Uddin, Mathematics and Computers in Simulation, 80 (7), 1509-1519 (2010).

[31] Cazzola, E., M. E. Innocenti, S. Markidis, M. V. Goldman, D. L. Newman, and G. Lapenta, Physics of Plasmas (1994-present), 22 (9), 092,901 (2015).

[32] Cazzola, E., M. E. Innocenti, M. V. Goldman, D. L. Newman, S. Markidis, and G. Lapenta, Geophys. Res. Lett., 43, 7840–7849, doi:10.1002/2016GL070195 (2016).

[33] Pritchett, P., Journal of Geophysical Research: Space Physics, 113, A6, (2015).

[34] Daughton,W., V. Roytershteyn, H. Karimabadi, L. Yin, B. J. Albright, B. Bergen, and K. J. Bowers, Nat. Phys., 7, 539–542, doi:10.1038/nphys1965 (2011); Zhou, M., X. H. Deng, and S. Y. Huang, Phys. Plasmas, 19, 042902, doi:10.1063/1.3700194 (2012).

[35] Zenitani, S., M. Hesse, A. Klimas, and M. Kuznetsova, Phys. Rev. Lett., 106, 195003, doi:10.1103/PhysRevLett.106.195003 (2011).

[36] Dunlop, M. W., A. Balogh, K.-H. Glassmeier, and P. Robert, J. Geophys. Res., 107(A11), 1384, doi:10.1029/2001JA005088 (2002).

[37] Goldman, M.V., D.L. Newman, G. Lapenta, *Space Sci. Rev.*, DOI 10.1007/s11214-015-0154-y (2015).

[38] Swisdak, M., Geophys. Res. Lett., 43, 43-49, doi:10.1002/2015GL066980 (2016).

[39] Norgren, C., et al., Geophys. Res. Lett., 43, 6724-6733, doi:10.1002/2016GL069205 (2016).

[40] Lavraud, B., et al., Geophys. Res. Lett., 43, doi:10.1002/2016GL068359 (2016).

[41] Pritchett, P. L., J. Geophys. Res., 106, 3783 (2001)

[42] Eriksson, S., et al., Phys. Rev. Lett., doi:10.1103/PhysRevLett.117.015001 (2016)

Figures

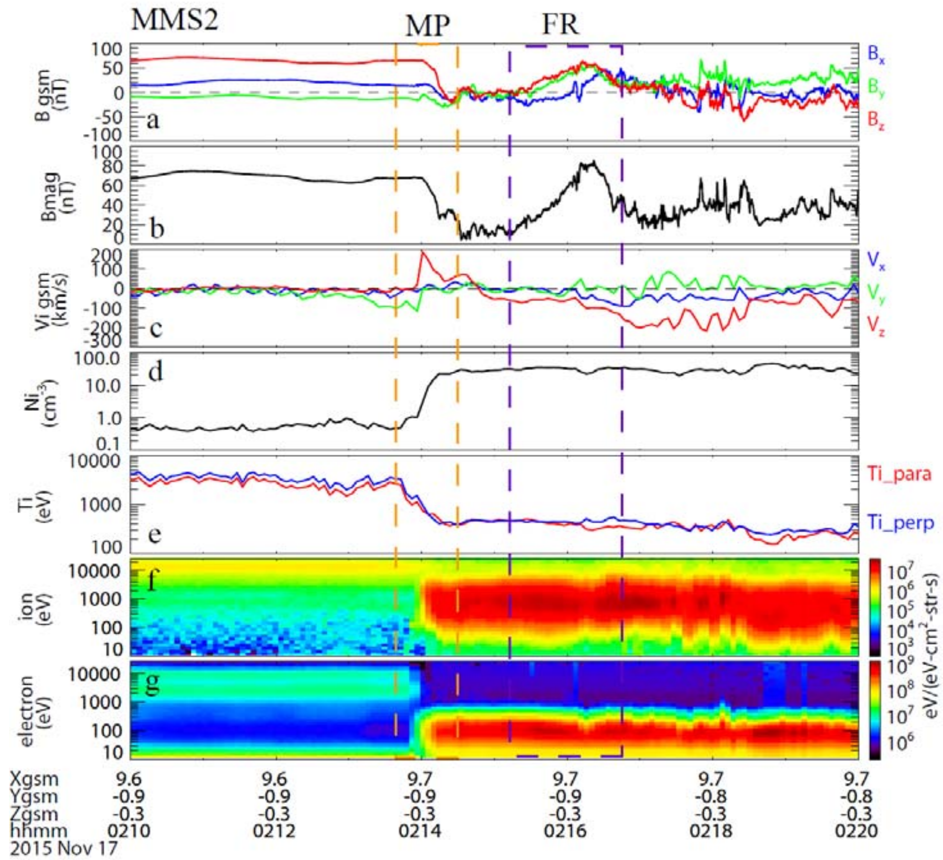

FIG. 1. Overview of MMS2 observations between 02:10 and 02:20 UT. From the top to bottom are: (a) magnetic field vectors, (b) magnetic field strength, (c) ion bulk velocity, (d) ion density, (e) ion parallel (red) and perpendicular temperatures (blue), (f) ion and (g) electron differential energy fluxes. All vectors are in GSM coordinates.

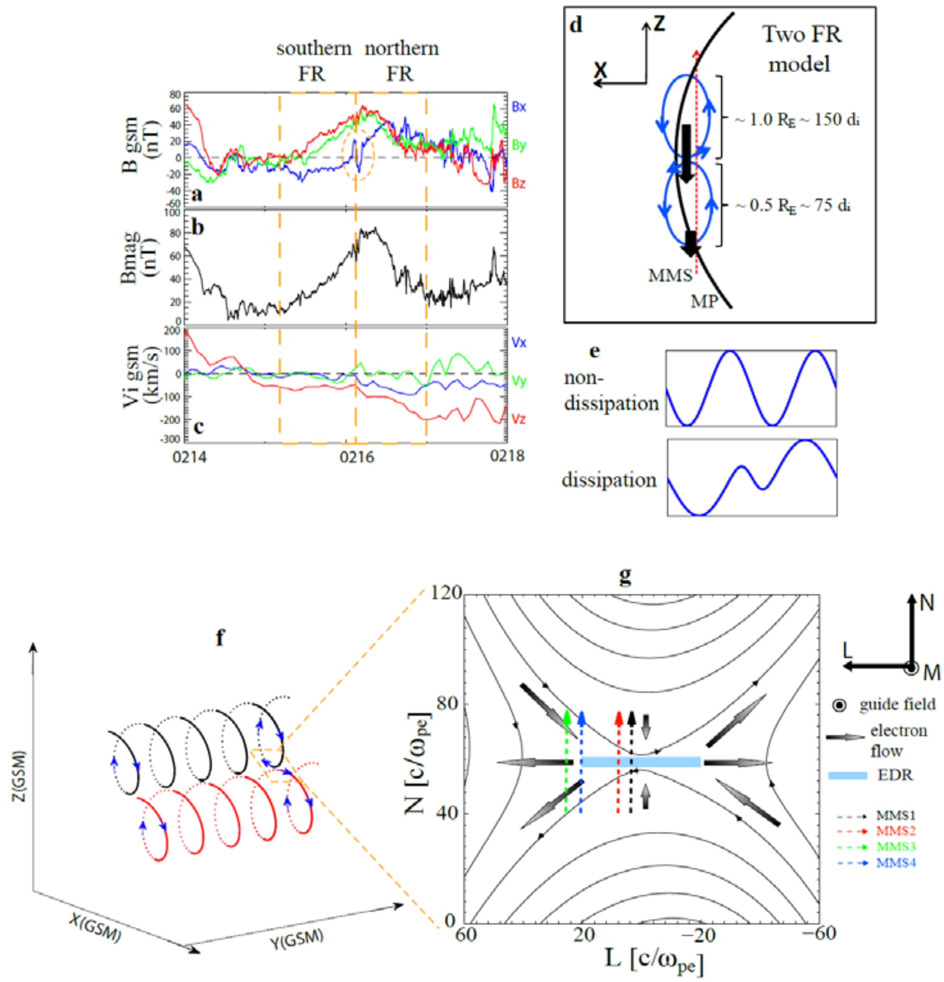

FIG. 2. (a)-(c) show the magnetic field and ion bulk velocity observed by MMS2 between 02:14 and 02:18 UT. (d) is a schematic of MMS orbits relative to the MP and FRs. (e) depicts the variations of B_x recorded by the virtual MMS spacecraft shown in (d) for two different cases: the upper panel is the case without dissipation while the lower panel is the case with dissipation between the two FRs. (f) is a 3-D schematic of field lines of two FRs in GSM coordinates, (g) is a zoomed-in 2D view of FR coalescence and MMS configuration in the L-N plane.

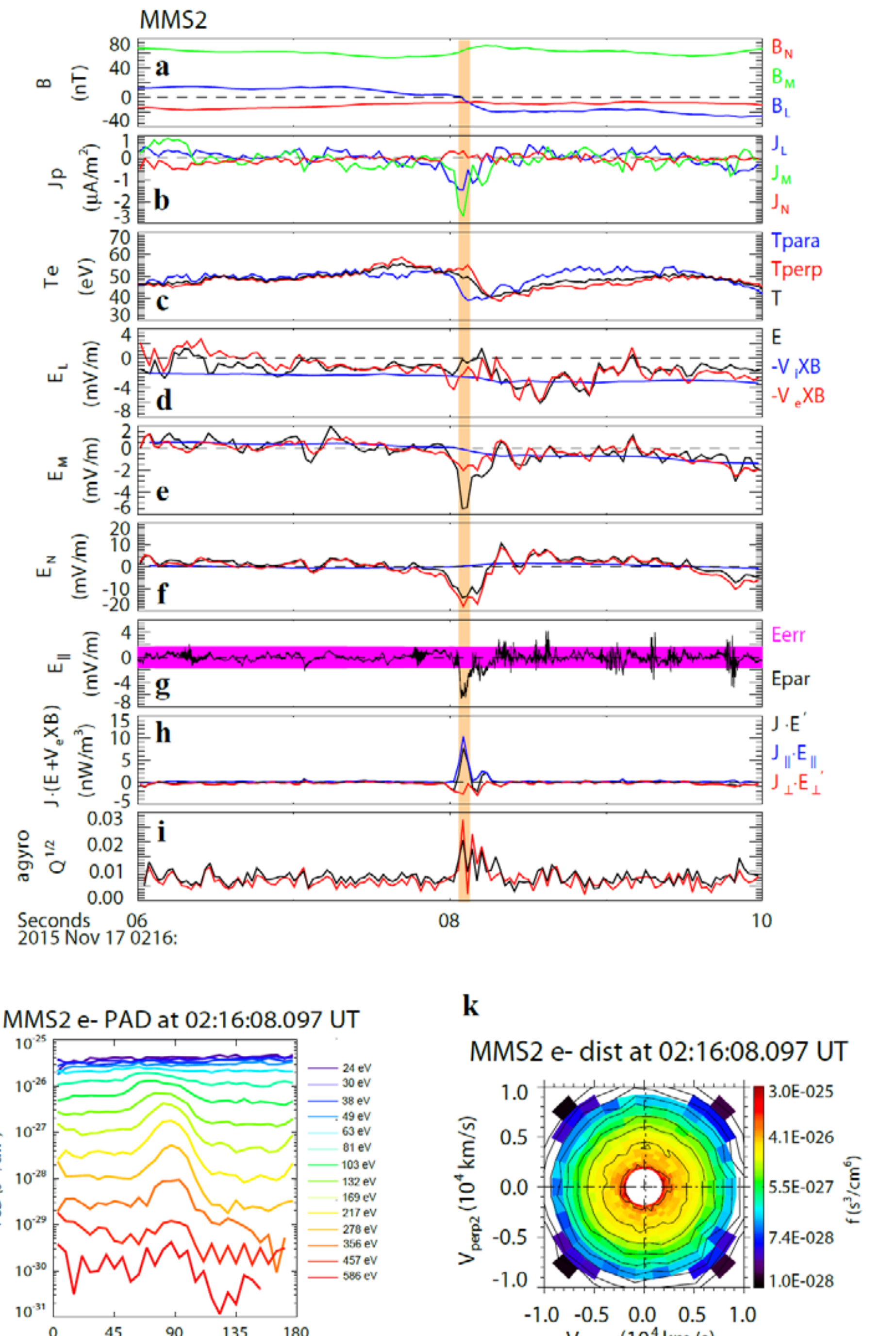

FIG. 3. Electron-scale layer embedded within the merging sheet. (a) magnetic field, (b) current density, (c) electron parallel (blue), perpendicular (red) and average (black) temperatures, (d)-(f) comparison of the three components of the measured electric field (black), $-\mathbf{V}_i\times\mathbf{B}$ (blue) and $-\mathbf{V}_e\times\mathbf{B}$ (red), (g) parallel electric field, magenta shading indicates the errors associated with the measurements, (h) $\mathbf{J}\cdot\mathbf{E}'=\mathrm{J}\cdot(\mathbf{E}+\mathbf{V}_e\times\mathbf{B})$ and (i) a measure of electron nongyrotropy. Red and black traces

indicate the values that were calculated by using the upper and lower limit of the measured pressure, respectively. Orange shading marks the electron-scale layer with significant $E_{||}$ ($|E_{||}|$ is larger than the error bar), (j) electron PAD and (k) electron velocity distribution in the plane perpendicular to the magnetic field within the electron-scale layer.

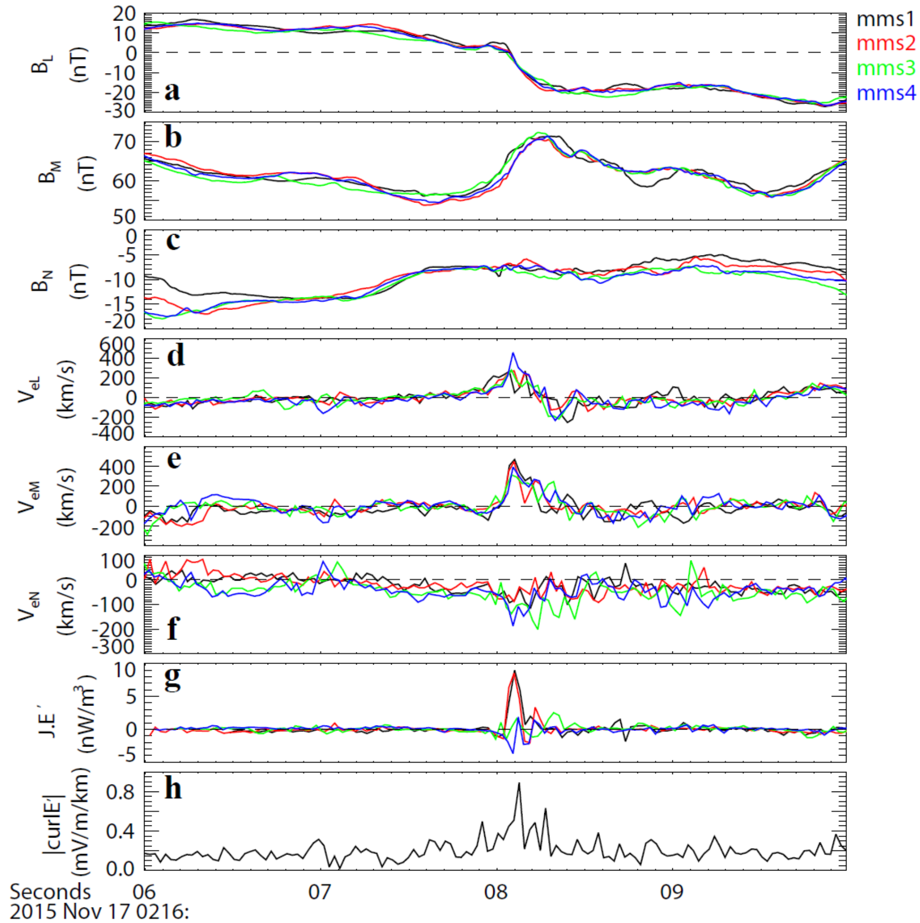

FIG. 4. Four spacecraft observations around the EDR. Magnetic fields: (a) B_L, (b) B_M, (c) B_N, electron flow: (d) V_{eL}, (e) V_{eM}, (f) V_{eN}, (g) $J\cdot(E+V_e\times B)$ and (h) $|\nabla\times(E+V_e\times B)|$.